

## Altered gene expression related to fuel use and sensory capacity in tanycytes throughout the hibernation season in the golden hamster

Journal:	<i>Canadian Journal of Zoology</i>
Manuscript ID	cjz-2024-0180.R2
Manuscript Type:	Research Article
Date Submitted by the Author:	27-Mar-2025
Complete List of Authors:	Melum, Vebjørn; UiT The Arctic University of Norway, Arctic Seasonal Timekeeping Initiative (ASTI), Arctic Chronobiology and Physiology research group, Department of Arctic and Marine Biology; University of Strasbourg, Institute of Cellular and Integrative Neurosciences Bothorel, Béatrice; University of Strasbourg, Institute of Cellular and Integrative Neurosciences Moralia, Marie-Azélie; University of Strasbourg, Institute of Cellular and Integrative Neurosciences Simonneaux, Valerie; University of Strasbourg, Institute of Cellular and Integrative Neurosciences Hazlerigg, David; UiT The Arctic University of Norway, Arctic Seasonal Timekeeping Initiative (ASTI), Arctic Chronobiology and Physiology research group, Department of Arctic and Marine Biology Wood, Shona; UiT The Arctic University of Norway, Arctic Seasonal Timekeeping Initiative (ASTI), Arctic Chronobiology and Physiology research group, Department of Arctic and Marine Biology
Is the manuscript for consideration in a Special Issue or Collection?:	17th International Hibernation Symposium Collection
Keyword:	tanycyte, hibernation, torpor, seasonal, photoperiod, refractory, <i>Mesocricetus auratus</i>

SCHOLARONE™  
Manuscripts

1 **Altered gene expression related to fuel use and sensory capacity in tanycytes throughout the**  
2 **hibernation season in the golden hamster**

3 Vebjørn. J. Melum<sup>1,2</sup>, Béatrice Bothorel<sup>2</sup>, Marie-Azélie Moralia<sup>2</sup>, Valérie Simonneaux<sup>2</sup>, David  
4 G. Hazlerigg<sup>1</sup>, Shona H. Wood<sup>1</sup>

5 1 UiT — The Arctic University of Norway, Department of Arctic and Marine Biology, Arctic  
6 Chronobiology and Physiology research group, Tromsø, Norway

7 2 University of Strasbourg, Institute of Cellular and Integrative Neurosciences, Strasbourg,  
8 France

Draft

## 9 Abstract

10 Hibernation is a physiological and behavioural adaptation that permits survival during periods  
11 of reduced food availability and extreme environmental temperatures. This is achieved through  
12 episodes of metabolic depression and body cooling (torpor), and subsequent rewarming  
13 (arousal), cycling between which is presumed to stem from changes in hypothalamic metabolic  
14 control. Several recent lines of evidence implicate the hypothalamic tanycytes in this  
15 phenomenon.

16 To investigate tanycytic changes over the hibernation season, golden hamsters (*Mesocricetus*  
17 *auratus* (Waterhouse, 1839)), were transferred from long photoperiod 22°C to short  
18 photoperiod (SP) 8°C, sampling animals at physiologically defined points across the  
19 hibernation season for LASER capture microdissection and RNAseq of the tanycytic region.

20 Our analysis revealed a marked reduction in the expression of genes linked to ciliary assembly  
21 and GPCR-signalling during the hibernation season, as well as evidence for a shift towards  
22 increased glycolytic metabolism. These aspects were all reversed in refractory animals which  
23 spontaneously ceased to express torpor after extended exposure to SP 8°C. Tanycytes sampled  
24 mid-torpor show increased expression of immediate-early genes compared to the interbout  
25 euthermic state, while genes linked to RNA processing and translation show the reverse effect.

26 The implications of these findings for the putative involvement of tanycytes in hibernation  
27 control mechanisms are discussed.

28 **Keywords:** Tanycyte, hibernation, torpor, seasonal, photoperiod, refractory, hamster,  
29 *Mesocricetus auratus*

30

## 31 **Introduction**

32 Hibernation is a physiological and behavioural adaptation that permits survival during seasonal  
33 periods of energy shortage *via* a combination of pre-hibernal energy storage and hibernal  
34 metabolic depression (torpor). Ground squirrels, dormice and golden/European hamsters are  
35 examples of deep hibernators, all requiring a seasonal preparative phase to express the  
36 hibernation phenotype. Torpor during deep hibernation can reduce metabolic rate to 1% of the  
37 active state (reviewed in: (Ruf and Geiser 2015)). Animals undergoing deep hibernation  
38 repeatedly cycle between the hibernating (torpid) and the active (aroused) states for the entire  
39 hibernation season (T-A cycling). The seasonal decline in photoperiod is the primary cue used  
40 to initiate the suite of seasonal physiological changes to permit the expression of the hibernation  
41 phenotype. In a lab setting, it is possible to induce the physiological preparations for deep  
42 hibernation in golden hamsters (*Mesocricetus auratus* (Waterhouse, 1839)) by transferring  
43 them from long (LP) to short photoperiods (SP). Exposure to SP results in sexual quiescence,  
44 brown adipose tissue recruitment, moderate fattening and food caching over a period of 8 weeks  
45 (Lyman et al. 1982; Markussen et al. 2024). SP-adapted animals exposed to a reduced ambient  
46 temperature (8°C) express T-A cycling for several months (Lyman et al. 1982; Markussen et  
47 al. 2024). Finally, there is a spontaneous termination of T-A cycling concomitant with  
48 physiological preparations for the coming spring including reactivation of the gonads. This is  
49 referred to as the refractory state (Sáenz de Miera et al. 2014). Importantly, the refractory state  
50 occurs spontaneously, independent of changes in ambient temperature or photoperiod,  
51 signifying the existence of an internal timing mechanism (circannual clock), which would be  
52 an advantage to an animal isolated in a hibernaculum (Gwinner 1986; Hut et al. 2014; Sáenz de  
53 Miera et al. 2014). Golden hamsters are defined as a type I circannual species, meaning only  
54 the exit from the hibernation state is spontaneous, whereas the preparation for hibernation  
55 requires a declining photoperiod signal (Dunlap et al. 2004) (and reviewed in: (Hazlerigg et al.

56 2023)). Hence, we may in summary identify 3 key regulatory aspects governing the hibernation  
57 season: (i) The regulation of the preparative events to allow entry into torpor and subsequent  
58 rounds of T-A cycling, (ii) the regulation of the T-A cycle itself, and (iii) the termination of the  
59 hibernation season through the development of the refractory state.

60 Recent studies in mammals suggest that a specialised glial cell type present in the ependymal  
61 region surrounding the third ventricle in the mediobasal hypothalamus, the tanycyte, may play  
62 a key role in all the above aspects. Tanycytes sit in a privileged position in the mediobasal  
63 hypothalamus, forming the interface between the blood brain barrier and the cerebrospinal fluid  
64 (CSF)-brain barrier. There, they are thought to act as metabolic sensors controlling the access  
65 of nutrients and hormones to the brain (Parkash et al. 2015; Bolborea et al. 2020; Duquenne et  
66 al. 2021; Lhomme et al. 2021).

67 It has also become abundantly clear over the last two decades that tanycytes play a key role in  
68 driving seasonal photoperiodic changes in metabolic and reproductive physiology through  
69 modulation of hypothalamic thyroid hormone (TH) availability (reviewed in: (Dardente et al.  
70 2014, 2019; Hazlerigg and Simonneaux 2015)). This process depends on photoperiod, with  
71 melatonin duration as the primary cue used to initiate the programme of seasonally adapted  
72 physiological change. Melatonin acts via MT1 receptors in the *pars tuberalis* (PT) to control  
73 photoperiod-dependent production of the glycoprotein hormone, thyrotropin (TSH), which in  
74 turn acts on TSH receptor (TSH-R)-expressing tanycytes (Hanon et al. 2008, 2010; Sáenz de  
75 Miera et al. 2013; Wood et al. 2020). In response to LP, TSH is produced and tanycytes convert  
76 inactive thyroxine (T4) to active triiodothyronine (T3) via a deiodinase enzyme (DIO2). On SP,  
77 when TSH synthesis is inhibited, increased DIO3 reduces T3 to 3,5-diiodo-L-thyronine (T2).  
78 Infusion of TSH into the 3<sup>rd</sup> ventricle of an SP golden hamster increases Dio2 expression and  
79 restores its summer phenotype within 4-6 weeks (Klosen et al. 2013). Furthermore,  
80 experimental manipulation of TH status in Siberian hamsters (*Phodopus sungorus*, (Pallas,

81 1773)) revealed that a hypothyroid environment is permissive for the expression of daily torpor  
82 and that T3 manipulation can reversibly halt torpor (Murphy et al. 2012; Bank et al. 2015,  
83 2017). Studies manipulating T3 have not been reported in a deep hibernator, but it is likely that  
84 the low TH environment within the hypothalamus and subsequent effects on the reproductive  
85 axis are permissive for hibernation (Gaston and Menaker 1967; Morin and Zucker 1978;  
86 Darrow et al. 1987).

87 Analyses of brain c-Fos expression pattern (a marker for cellular activation) demonstrate that  
88 in both 13-lined ground squirrels (*Ictidomys tridecemlineatus*, (Mitchill, 1821)) and in golden  
89 hamsters tanycytes show dramatic changes in activation over the T-A cycle (Bratincsák et al.  
90 2007; Markussen et al. 2024). We have previously suggested that tanycytes, through their  
91 sensitivity to factors in the blood or cerebrospinal fluid, may mediate metabolic feedback-based  
92 initiation of the spontaneous arousal process and that the observed cellular activation during T-  
93 A cycling relates to this function (Markussen et al. 2024).

94 Finally, in several seasonal models, including hibernators (European hamster (*Cricetus cricetus*  
95 (Linnaeus, 1758)), Arctic ground squirrel (*Urocitellus parryii* (Richardson, 1825)) and golden  
96 hamster), it has become clear that tanycytic changes in deiodinase expression occur  
97 spontaneously with the onset of the refractory state (Revel et al. 2006; Sáenz de Miera et al.  
98 2013, 2014; Milesi et al. 2017; Chmura et al. 2022). This suggests that, as well as regulating  
99 photoperiod-dependent preparation of winter physiology, tanycytes may also drive innately  
100 timed spontaneous termination of the winter hibernating state (Hut et al. 2014; Sáenz de Miera  
101 et al. 2014).

102 Based upon these studies implicating tanycytes in the regulation of hibernation, the aim of this  
103 study was to characterise changes in tanycyte characteristics over the course of the hibernation  
104 season. For this purpose, we chose the golden hamster as a model, since all three aspects of  
105 hibernation regulation (photoperiodic induction, T-A cycling and the refractory state) are

106 strongly expressed in this species. Here, we describe changing characteristics at the  
107 transcriptome level based on RNAseq analysis of LASER capture microdissected tissue  
108 samples taken before, during and after the hibernation phase as well as from torpid and aroused  
109 animals in the middle of the hibernation phase.

Draft

OPEN ACCESS: This work (the Author's Accepted Manuscript) is licensed under a Creative Commons Attribution 4.0 International License (CC BY 4.0), which permits unrestricted use, distribution, and reproduction in any medium, provided the original author(s) and source are credited.

## 110 **Materials and Methods**

### 111 *Animals*

112 Three months old male golden hamsters (*Mesocricetus auratus*) were housed under long  
113 photoperiod (LP, 14 hours of light, 10 hours of dark) and an ambient temperature of 22°C.  
114 Animals had *ad libitum* access to food and water throughout the experiment and received  
115 nesting material and a wooden stick in their home cage. Three weeks prior to the experiment,  
116 under isoflurane anesthesia, an iButton (Maxim) was implanted to record body temperature.  
117 Prior to implantation iButtons were coated in 3 layers of paraffin/Elvax coating  
118 (Respironics/Mini Mitter, Bend, OR) and sterilised. Each animal was anesthetized by 3%  
119 isoflurane, surgery was performed under 3% isoflurane and 95% oxygen. The iButton was  
120 implanted in the abdominal cavity by laparotomy. At the site of laparotomy a subcutaneous  
121 injection of lidocaine mixture (lurocaine/bupivacaine, 2.5 mg/kg each) was administered.  
122 Subcutaneous injection of meloxicam (2 mg/kg) was performed while the animal is  
123 anesthetised, and following surgery meloxicam (metacam® buvable 1.5 mg / ml, dose 1 mg /  
124 kg) was added to drinking water 3 days post-surgery. Drinking was monitored in the animals  
125 post-surgery establishing that they were drinking normally.

126

127 At the start of the experiment, six groups ( $n = 5$  to 6 per group) were kept on LP at 22°C. The  
128 LP group was sampled 16 weeks into the experiment to age match the SP animals. The  
129 remaining animals were transferred to short photoperiod (SP, 10 hours of light/14 hours of dark)  
130 at an ambient temperature of 8°C to initiate hibernation. Based on the regression of the testis  
131 we defined animals as “pre-hibernators” and sampled 4 weeks after transfer to SP (pre-  
132 hibernation), after 8 to 12 weeks of SP prior to initiating T-A cycling (late pre-hibernation).  
133 After three T-A cycles either when aroused in interbout euthermic (IBE) or in deep torpor  
134 (torpid) we sampled animals. The average IBE duration in this experiment was approximately

135 24 hours, animals were sampled late in their interbout euthermia phase (23 hours). The average  
136 torpor duration in this experiment was approximately 26 hours and torpid animals were sampled  
137 at their mid-point of torpor. After approximately 20 weeks of SP exposure, animals  
138 spontaneously stopped hibernating and were sampled at least 2 weeks after the last torpor bout  
139 (refractory).

140 For sampling, animals were anaesthetised with 4% isoflurane and decapitated. The study was  
141 conducted at the Chronobiotron (CNRS- UMS 3415) in accordance with the French National  
142 Law implementing the European Communities Council Directive 2010/63/EU and the French  
143 Directive 2013-118. Animal procedures were reviewed by the local ethical committee (Comité  
144 Régional d'Éthique en Matière d'Expérimentation Animale de Strasbourg, CEEA 35) and the  
145 official authorization was given on December 2019 by la Direction Générale de la Recherche  
146 et de l'Innovation under the number APAFIS#22534-2019100822522580 v2.

#### 147 *Plasma samples*

148 At euthanasia, blood was collected in tubes with heparin, inverted and wrapped in aluminium  
149 foil to protect it from light. The blood was allowed to clot for 20 minutes on ice before moved  
150 to a precooled centrifuge at 4 °C and centrifuged for 20 minutes for euthermic animals and 50  
151 minutes for torpid animals at 2000 G. The time span was required to obtain a clear separation  
152 of plasma and blood cells in the torpid group. Plasma was collected in aliquots and stored at -  
153 80°C until further use.

154 Testosterone concentration in the plasma sample was measured with a competitive inhibition  
155 ELISA kit (MyBioSource, MBS2516160, USA) following manufacturer's instructions, and  
156 optical density was measured by a microplate reader (Promega Glomax explorer GM3510) at  
157 450 nm.

158 *Tissue collection*

159 After decapitation, the brain was carefully removed from the skull by one operator, while  
160 another placed the animal on its belly and proceeded with tissue collection. The interscapular  
161 adipose tissue (iAT), containing both interscapular brown adipose tissue (iBAT) and  
162 interscapular subcutaneous white adipose tissue (iWAT) was removed. The iAT was weighed  
163 and visible iBAT was dissected, and the remaining iWAT was weighed. iBAT mass = iAT mass  
164 - iWAT. Testes were dissected out and weighed to confirm reproductive status.

165 *LASER capture microdissection and RNA extraction*

166 The brains were covered with pre-cooled OCT, snap frozen in chilled isopentane over dry ice  
167 and 95% ethanol and stored at -80°C. Each brain was cut, with a cryostat (-20°C; CM3050 S,  
168 Leica Biosystems), in series of 20 µm thick sections covering the whole medio-basal  
169 hypothalamic region (Bregma -1.8 mm to -3.2 mm) and mounted on 6-8 membrane slides  
170 (415190-9081-000, Carl Zeiss) of 8 sections each. Slides were stored at - 80°C until further use.  
171 Immediately before LASER capture microdissection (LCMD), the membrane slides were  
172 stained using cresyl violet as described previously (Melum et al. 2024). When ready, the slides  
173 were transferred to the LASER micro dissector (PALM MicroBeam system, Zeiss) with the  
174 PALMRobo software (V4.8, Zeiss) and microdissection was completed within 45 minutes to  
175 minimize RNA degradation. LCMD was carried out at 10x, with the following settings: Cut  
176 energy = 42-49; Cut focus = 84; LPC Energy = 58; LPC focus = 84. To capture a tanycyte-  
177 enriched sample and minimise the amount of ependymal cells we limited the dorso-ventral  
178 extent of the area captured to two times the width of the pars tuberalis (PT) per section. Based  
179 on our previous study this measure can correct for individual animal size differences and  
180 changes in the extent of the tanycytic region as the sections cover the rostro-caudal extent  
181 (Melum et al. 2024). The width of the area captured was only two to three cell bodies thick to  
182 further enrich for tanycytes which closely line the 3<sup>rd</sup> ventricle (Supplementary Figure 1A).

183 While this approach will not give a pure tanycyte sample it will be greatly enriched for tanycytes  
184 compared to previous studies of this region using the entire medio-basal hypothalamus (Haugg  
185 et al. 2022). The tanycyte-enriched samples were collected on to microdissection caps (415190-  
186 9211-000, Carl Zeiss), snap frozen on dry ice and stored at  $-80^{\circ}\text{C}$ . The RNA was extracted from  
187 the microdissected tissue using the Qiagen all prep DNA/RNA micro kit (80284) following the  
188 supplied instructions. The RNA integrity numbers were determined by TapeStation high  
189 sensitivity RNA analysis (5067-5579, 5067-5581, 5067-5580, Agilent) and all used samples  
190 had a RNA integrity numbers (RIN) between 7 to 9.

#### 191 *LCMD-RNAseq, mapping and gene counts*

192 RNA-seq library construction was performed by BGI using their standard RNAseq protocol  
193 and Illumina high seq 4000. Quality control checks and barcode removal were performed  
194 according to the BGI protocol. Approximately 35-40 million reads per sample were generated.  
195 Mapping was performed using STARaligner and the standard settings (Dobin et al. 2013).  
196 Reads were mapped to the golden hamster genome (BCM\_Maur\_2.0, ref.seq:  
197 GCF\_017639785.1) and the annotation was provided by NCBI  
198 (GCF\_017639785.1\_BCM\_Maur\_2.0\_genomic.gtf). The mapping rate was 88%. Feature  
199 counts was used to count the mapped reads to genes, using these parameters: featureCounts -p  
200 -t exon -g gene\_id, on average 70% of alignments were assigned to an annotated feature.

201 FASTQ files and count files were deposited in GEO under this accession  
202 identifier: GSE281814

#### 203 *Gene expression analysis*

204 We determined the median counts per million (CPM) across the whole experiment for each  
205 gene and applied a cut off of 10 raw counts, removing genes with a median of less than 0.5  
206 CPM from the analysis. 16 315 genes remained representing our LCMD transcriptome, this

207 dataset was used in all subsequent analysis. Three samples were excluded from the RNAseq  
208 analysis because they had low read counts and/or low RIN values and formed outliers in the  
209 initial data quality PCA analysis. In the final RNAseq analysis the numbers of animals for each  
210 group analysis were  $n=6$  in Prehib; Torpid; LP and  $n=5$  in Late Prehib; IBE; Refractory.  
211 Significance in this study was defined as a false discovery rate below 0.05.

212 To establish that we had a tanycyte-enriched sample, as in our previous study (Melum et al.  
213 2024), we used a single nuclei RNA-seq dataset which determined cell type specific markers  
214 for genes in the hypothalamus (Campbell et al. 2017). Using this list, we categorize the genes  
215 expressed in our dataset into cell types. We averaged the counts per million across the  
216 experiment for the genes in those specific cell type clusters and plotted the data to show cell  
217 type enrichment in our dataset (Supplementary Figure 1B).

218 Differential expression analysis of the RNAseq data were performed in R, with the Rstudio  
219 interface, using the EdgeR package (McCarthy et al. 2012; Chen et al. 2014; Zhou et al. 2014).  
220 In brief, a generalized linear model (GLM) analysis following the EdgeR manual was  
221 performed to determine which genes were differentially expressed between the groups. All  
222 genes with an *FDR* less than 0.05 were used in a PCA analysis using the package PCAtools  
223 (Blighe and Lun 2019). The same genes were plotted as a heatmap with five clusters (k-means)  
224 with the use of the package ComplexHeatmap (Gu et al. 2016). Enrichment analysis on each  
225 cluster was performed using ShinyGO (Ge et al. 2020) using GOterms, Kyoto encyclopedia of  
226 genes and genomes (KEGG) (Kanehisa & Goto 2000) and Reactome pathways. Fold  
227 enrichment refers to the percentage of genes in our list belonging to a specific pathway or a  
228 term, divided by the corresponding percentage in the background genome. Therefore, fold  
229 enrichment represents the over-representation of genes within a certain term or pathway, and  
230 the false discovery rate (*FDR*) is how likely this over-representation occurs by chance.

231 ShinyGO automatically removes redundant terms and pathways, the top terms/pathways are  
232 displayed in the figures and full results are in Supplementary Tables 2 and 4.

233 The package EnhancedVolcano (Blighe K, Rana S 2024) was used to make a volcano plot of  
234 genes upregulated in the IBE and Torpid states, with an *FDR* cut off of 0.05 and no log<sub>2</sub>-fold  
235 change cut off.

### 236 *Other statistical analysis*

237 Core body temperature data from iButtons (Maxim) were handled and analysed in R, with the  
238 Rstudio interface using the Tidyverse (Wickham et al. 2019) package. Graphpad prism was  
239 used to analyse and plot the mean core body temperature data, iBAT, testes mass and plasma  
240 testosterone concentration. One-way ANOVA and a Tukey test for multiple comparison was  
241 used. P value less than 0.05 were considered significant.

242 All scripts used to generate the figures are available in our github repository:  
243 <https://github.com/ShonaWood/SeasonalTanycytes>

## 244 **Results**

### 245 *Physiological responses over the course of a short-photoperiod induced hibernation season*

246 Our protocol for induction of a hibernation season in golden hamsters involves transferring  
247 animals from LP 22°C to SP 8°C (Figure 1A). In line with our published work, this initiates a  
248 shift towards an Autumn/Winter program, first shutting down the reproductive axis (Figure 1  
249 A, D, E), and entering a pre-hibernation state characterised by a downward adjustment of the  
250 core-body temperature ( $T_b$ ) and an increase in brown adipose tissue (BAT) (Figure 1A, B,  
251 C)(Chayama et al. 2016; Markussen et al. 2024). After approximately 8-12 weeks in SP 8°C T-  
252 A cycling commences, defined by multi-day bouts of torpor, during which  $T_b$  is close to ambient  
253 temperature (approximately 8°C), separated by spontaneous return to euthermic temperatures  
254 (interbout euthermia (IBE)) (Figure 1A). Then, after approximately 20 weeks in SP 8°C, the  
255 animals spontaneously cease to show T-A cycling and start to re-grow their testes (refractory  
256 state) (Figure 1A, D, E). The refractory state is associated with a progressive increase in  $T_b$  but  
257 this does not reach the  $T_b$  values recorded during LP (Figure 1B).

258

### 259 *Divergent gene expression dynamics in the tanycytic region over the course of the hibernation* 260 *season*

261 To assess how changes in tanycyte characteristics mirror hibernation status, we sampled  
262 animals from LP, SP 8°C 4 weeks (pre-hibernation), SP 8°C 8-12 weeks (late pre-hibernation),  
263 during hibernation (IBE and torpid), and finally once animals had entered the refractory state  
264 (Figure 1A). Using a LASER capture microdissection (LCMD) approach, we generated  
265 tanycyte-enriched samples (Melum et al. 2024) (Figure 1F and Supplementary Figure 1A) from  
266 each of our physiologically defined groups and these were then subjected to RNAseq.

267 Among the euthermic animals, we found that over 15% of all detectable transcripts showed  
268 significant changes in expression ( $FDR < 0.05$ ) over the whole experiment (seasonal  
269 differentially expressed genes (DEGs) (Supplementary Table 1). Performing a PCA analysis of  
270 the seasonal DEGs, shows that 76.8%, between sample variation in gene expression was  
271 accounted for by a single principal component, resolving samples according to seasonal status  
272 (Figure 1G).

273 Focusing on these seasonal DEGs, we used K-means hierarchical clustering to resolve five  
274 distinctive expression profiles showing different dynamics over the course of the hibernation  
275 season (Figure 2A). Genes constituting clusters 1 (388 genes) are characterised by high  
276 expression under LP which then declines upon exposure to SP. Cluster 1 genes maintain  
277 reduced expression under SP even in the refractory state. This suggests that cluster 1 genes  
278 represent a group whose expression is primarily dependent on photoperiodic input as opposed  
279 to seasonal hibernation status. In line with this view, two canonical photoperiod-regulated genes  
280 (*Aldh1a1* and *Dio2* (Hanon et al. 2008, 2010; Shearer et al. 2010)) are members of cluster 1  
281 (Figure 2B and Supplementary Table 1).

282 We used both Kyoto encyclopedia of genes and genomes (KEGG) and Reactome pathway  
283 analysis to gain insights into the likely functional consequences of observed changes in gene  
284 expression in clusters 1 - 5 (Supplementary table 2, Figure 2B). Cluster 1 shows strong pathway  
285 enrichment related to amino acid metabolism (3.92-fold enrichment, 0.00034  $FDR$ ), retinol  
286 metabolism (10.35-fold enrichment, 0.03  $FDR$ ), PPAR signalling pathway (7.25-fold  
287 enrichment,  $6.36 \times 10^{-5}$   $FDR$ ) and fatty acid metabolism (3.99-fold enrichment, 0.0029  $FDR$ ). A  
288 closer look at the PPAR pathway enriched genes (Supplementary Figure 1B) shows that  
289 lipogenesis and fatty acid transport related genes are highly expressed in LP, concurring with  
290 earlier work noting that tanycytes transport fatty acids and in combination with astrocytes  
291 regulate lipid metabolism (Hofmann et al. 2017). This pathway enrichment also reflects the

292 well documented direct effects of photoperiod in retinoic acid (RA) signalling in mammals  
293 (Shearer et al. 2010) (Supplementary Figure 1C).

294 Cluster 2 (463 genes) is defined by low expression in the pre-hibernation and hibernation  
295 animals and high expression in LP and refractory animals. This group shows strong pathway  
296 enrichment for neurotransmitter uptake in glial cells and G-protein coupled receptor (GPCR)  
297 ligand binding (Figure 2B and Supplementary Table 2), echoing our previous work describing  
298 strong photoperiodic effects on ciliation in the tanycytic region of Siberian hamsters (Melum et  
299 al. 2024). Consistent with this, we found strong enrichment of GO terms linked to ciliary  
300 function (Figure 2C and Supplementary Table 2), and the expression patterns for key cilia genes  
301 (*Tubb4b*, *Cfap20*, *Cfap47*) nicely demonstrate the cluster 2 expression pattern (Figure 2A).

302 Cluster 3 (233 genes) does not show a strong overall seasonal expression trend, but a lower  
303 expression in the mid-hibernation season (IBE) state compared to either the late-pre-hibernation  
304 state or in the refractory state (Figure 2A). This was the smallest cluster and is enriched for  
305 neurotransmitter recycling and synapse pathways (Figure 2B and Supplementary Table 2). GO  
306 term analysis also revealed genes involved in clathrin sculpted vesicles (*Gad1*, *Gad2*, *Rab3a*)  
307 (Supplementary Table 2 and Figure 2B), which have been proposed to be important in the  
308 communication of tanycytes to neurons (Pasquettaz et al. 2021).

309 Genes constituting Clusters 4 (545 genes) and 5 (566 genes) are characterised by low levels of  
310 expression in LP, which then increase upon exposure to SP and entry into the hibernation phase,  
311 before a subsequent decline in the refractory state (Figure 2A). These two clusters differ from  
312 one another in that declining expression is seen earlier in cluster 4, when animals are still  
313 undergoing T-A cycling, than in cluster 5, in which a decline in expression occurs in the  
314 refractory state (Figure 2A).

315 Cluster 4 shows pathway enrichment linked to mitogen-activated protein kinase (MAPK)  
316 signalling and calcium signalling as defining the pre-hibernation state (Figure 2B). The MAPK  
317 transduction pathway relates to cell growth, division and differentiation, suggesting  
318 remodelling of the tanycytic region in response to SP exposure. Consistent with this  
319 interpretation and previous descriptions of its expression dynamics in golden hamsters, Dio3 is  
320 a member of cluster 4 (Figure 2A )(Milesi et al. 2017). We also note that Slc2a5, a fructose  
321 transporter, is highly expressed in the pre-hibernation state, concomitant with a decrease in  
322 Slc2a1, a glucose transporter (Figure 2A, D and Supplementary Figure 2A).  
323 Phosphofructokinase (Pfkf), the key enzyme in glycolysis that catalyses the phosphorylation  
324 of fructose-6-phosphate is also a member of cluster 4, along with Gapdh and Eno2, all  
325 important members of the glycolysis pathway (Figure 2A, D).

326 Cluster 5, constituting genes whose expression is increased during the hibernation season and  
327 then decline in the refractory state, is strongly enriched for “metabolism” pathways (Figure 2B)  
328 and the GO terms relating to catabolic processes and oxidoreductase activity (Supplementary  
329 Table 2). Specifically, genes relating to the pathways; Glycine, serine and threonine metabolism  
330 and carbohydrate metabolism show increased expression in the hibernation season (Figure 2B),  
331 as do several genes linked to glycolysis (Adpgk, Tpi1, Pkg1, Pck2, Ldhd) (Figure 2D).  
332 Similarly key elements of glucose-6-phosphatase activity including catalytic subunit 3 (G6pc3),  
333 Slc37a4 (G6pt), and Adpgk, are found in cluster 5 (Figure 2A, D). We also note that glycogen  
334 phosphorylase (Pgym), which breaks down glycogen was present in cluster 5, suggesting  
335 depletion of glycogen stores in preparation for, and, during hibernation (Figure 2A,  
336 Supplementary Figure 2B), potentially to supply neurons with glucose via the G6pase system  
337 (Barahona et al. 2024).

338 *Immediate early gene expression and RNA splicing during torpor*

339 To investigate the differences in our tanycyte-enriched samples between torpid and interbout  
340 euthermic states, we performed RNASeq on animals at the mid-point of torpor (average 13.3  
341 hours) at a  $T_b$  of 8°C and contrasted the expression profile with that of IBE animals (Figure  
342 3A). This revealed 1674 DEGs ( $FDR < 0.05$ ), 668 of which were increased during torpor (Figure  
343 3B and Supplementary Table 3). We noted that a striking number of immediate early genes  
344 were increased during torpor (including c-Fos, Jun, Junb, Egr1) (Figure 3B and C), with c-Fos  
345 showing the most impressive induction in terms of counts per million (Figure 3C). Also,  
346 amongst the most highly expressed genes during torpor were the RNA splicing/processing  
347 genes; Srsf5 and Pnlsr (Figure 3B), reflected in the pathway and GOterm enrichment analysis  
348 which showed strong enrichment for RNA splicing (Figure 3D and Supplementary Table 4).  
349 Furthermore, pathway analysis also revealed high expression of genes related to the cellular  
350 response to hypoxia during torpor (Figure 3D). Wsb1, a target of HIF1, with links to glucose  
351 and TH metabolism (Dentice et al. 2005; Haque et al. 2016), is increased in torpor (Figure 3C).  
352 We also note a small increase of Dio3 during torpor that is mirrored by a small increase of Dio2  
353 during IBE (Figure 3B).

354 By focusing on IBE, we noted Eif5, a translation initiation factor, Dyrk1b, a kinase involved in  
355 double strand break repair and transcriptional silencing, Mlx, a BHLH-zip transcription factor,  
356 and Kctd21, a histone deacetylase (Figure 3B, C), were among the most increased DEGs  
357 (Figure 3B). GO Enrichment analysis indicated genes relating the RNA-induced silencing  
358 complex (RISC) and histone methyltransferase activity were increased during IBE (Figure 3E).  
359 Collectively these data suggest that translation, gene silencing via microRNAs, and epigenetic  
360 regulation processes are enhanced in the interbout euthermic phase.

## 362 Discussion

363 Motivated by an accumulating literature indicating that tanycytes play a core role in the  
364 regulation of energy homeostasis in mammals (Bolborea and Dale 2013; Langlet 2014; Rizzoti  
365 and Lovell-Badge 2017; Prevot et al. 2018; Dali et al. 2023), and that seasonal adjustments in  
366 metabolic physiology may be initiated by changes in tanycyte function (Ebling 2014; Lewis  
367 and Ebling 2017; Ebling and Lewis 2018; Dardente et al. 2019; Melum et al. 2024), we sought  
368 in the present study to characterise changes in tanycyte phenotype across the hibernation season  
369 in the golden hamster. To this end we undertook transcriptomic profiling of LCMD samples  
370 from the tanycytic region taken at specified points during the hibernation season defined by  
371 telemetric monitoring of  $T_b$ . Based on the reasonable assumption that changes in transcriptomic  
372 profile reflect underlying changes in cellular physiology the following inferences can be drawn  
373 about changes across the season as a whole:

374 Firstly, among the set of seasonal DEGs, fewer than 20% (cluster 1) appear to primarily be  
375 controlled by photoperiod as opposed to seasonal status. This demonstrates that while, in the  
376 golden hamster, the initiation of the hibernation season requires SP exposure, subsequent  
377 progression through the season from pre-hibernation to the refractory state constitutes an  
378 innately driven temporal sequence of events. The presence of *Dio2*, *Aldh1a1* and related genes  
379 in this photoperiod-regulated subset is consistent with the current consensus that nuclear  
380 hormone receptor signalling through thyroid hormone receptor (THR), retinoic acid and  
381 retinoid receptor (RAR-RXR) interactions, is central to photoperiodic triggering of changes in  
382 tanycyte function downstream of melatonin-dependent changes in TSH production by the PT  
383 (reviewed in: (Dardente et al. 2019)). The broader enrichment of this group for genes linked to  
384 amino acid and lipid metabolism is possibly an indicator of photoperiod-induced alterations of  
385 tanycyte-astrocyte communication to regulate lipid metabolism in the hypothalamus (Hofmann  
386 et al. 2017).

387 The second inference focuses on the larger group of DEGs that reflect the sequential seasonal  
388 state transitions (clusters 2, 4 and 5). Here, there is clear evidence for shifting metabolic fuel  
389 use within the tancytic region, with genes linked to fructose transport and glycolytic function  
390 showing higher expression during the pre-hibernation and hibernation state compared to LP or  
391 refractory states (Figure 2D). Use of the fructose pathway and endogenous production of  
392 fructose can shift an organism towards energy conservation with decreased mitochondrial  
393 activity and enhanced glycolytic activity, potentially representing an evolutionary conserved  
394 “survival” pathway (Johnson et al. 2020). Our data are consistent with a model in which  
395 tancytes undergo a photoperiod-driven/innately timed metabolic switch to conserve energy by  
396 shifting towards glycolysis and an enhanced use of tancyte glycogen stores. Photoperiodic  
397 regulation of genes involved in glycogen and glucose metabolism in tancytes of Siberian  
398 hamsters have also been reported (Nilaweera et al. 2011). This hypothesised shift in tancyte  
399 function would reduce tancytic energy requirements, and might enhance glucose supply to  
400 neighbouring cells via the glucose 6 phosphatase system (Barahona et al. 2024). This response  
401 can be seen as part of an organism-wide adjustment of fuel requirements to support hibernation,  
402 which is at the same time is highly tissue and brain region-specific (Williams et al. 2005;  
403 Schwartz et al. 2013; Vermillion et al. 2015).

404 Our third inference is that inverse to the above-mentioned changes in fuel metabolism, genes  
405 linked to the construction and function of cilia are a major feature of the seasonal DEGs. These  
406 show a marked decline in expression with the onset of the hibernation phase and then recovery  
407 to LP levels with the onset of the refractory state. Recently, we reported a similar result in  
408 juvenile Siberian hamsters, with exposure to SP during gestation and the juvenile period causing  
409 a significant reduction in the expression of ciliary gene expression and the numbers of cilia  
410 present on the ependymal surface in the basal 3<sup>rd</sup> ventricle (Melum et al. 2024). In both these  
411 studies, the described changes in ciliary gene expression are paralleled by changes in G-protein

412 coupled receptor (GPCR) gene expression, reflecting the role of cilia as scaffolds for cell-  
413 surface GPCRs to perform their signalling functions (reviewed in: (Schou et al. 2015)). Hence  
414 these results suggest that, in seasonal rodent species, the overwintering state may be  
415 characterised by reduced tancytic sensitivity to signals in the CSF bathing their apical surface.  
416 In addition to characterising transcriptomic change over the course of the hibernation season,  
417 we also compared the expression profiles of torpid and inter-bout euthermic animals. Echoing  
418 published *in situ* hybridization-based studies in golden hamsters and in hibernating ground  
419 squirrels (Bratincsák et al. 2007; Markussen et al. 2024), we saw a striking increase in the level  
420 of expression of c-Fos in the tancytic region of torpid animals. Moreover, this effect is seen  
421 for several other well-known immediate early genes (IEGs), including Egr1, Jun and Junb.  
422 These genes have been widely used as acute markers for cellular (and especially neuronal)  
423 activation in response to stimulatory signals acting through second messengers such as  
424 intracellular calcium or cAMP (reviewed in: (Lara Aparicio et al. 2022)). IEG acute sensitivity  
425 to stimulus relies on the fact that IEG response does not depend upon synthesis of other  
426 transcriptional regulators (reviewed in: (Bahrami and Drabløs 2016)). On this basis, the most  
427 obvious interpretation of our results is that increased IEG expression in torpor represents a  
428 tancytic response to stimulation. This raises the interesting issue of what stimuli are  
429 responsible for this effect. At the same time, we cannot exclude the possibility that the observed  
430 changes in IEG expression are a secondary consequence of changes in tancytic protein  
431 synthesis rate due to the low temperature in the torpid state. Since IEGs exhibit negative auto-  
432 regulation through transcriptional auto-repression (Gius et al. 1990), a general suppression of  
433 protein synthesis may lead to enhanced IEG transcription. Consistent with this interpretation,  
434 global suppression of translation during torpor and the resumption of protein synthesis in the  
435 inter-bout euthermic phase has been reported in 13-lined ground squirrels (Frerichs et al. 1998;  
436 Logan et al. 2019), and in the current study the expression of the translation initiation factor,

437 Eif5 was suppressed during torpor. Alternatively, given the highly brain region specific pattern  
438 of c-Fos induction during T-A cycling (Bratincsák et al. 2007; Fu et al. 2021; Markussen et al.  
439 2024; Haugg et al. 2024), a likely scenario is that the observed tancytic IEG response  
440 represents the actions of as yet unidentified local stimuli enhanced by suppression of  
441 translation-based autoregulatory feedback. Clearly further studies to isolate candidate stimuli  
442 and test their effects on tanycytes are now warranted.

443 Pathway analysis of DEGs with increased expression in torpor highlights the hypoxia response  
444 and effects on the control of RNA splicing, both of which have previously been implicated in  
445 hibernation physiology (Maistrovski et al. 2012; Sano et al. 2015; Fu et al. 2021). Notably,  
446 Wsb1 a HIF1- $\alpha$  induced gene (reviewed in: (Haque et al. 2016)) has been linked to  
447 ubiquitination, and hence targeted degradation of DIO2 (Dentice et al. 2005; Zavacki et al.  
448 2009). This suggests that TH metabolism may be modulated during T-A cycling by post-  
449 translational mechanisms. While exogenous T3 delivered to the hypothalamus blocks torpor in  
450 Siberian hamsters (Murphy et al. 2012; Bank et al. 2017), the equivalent experiment is yet to  
451 be conducted in a deep hibernator. Furthermore, measurement of deiodinase enzyme activity  
452 during a T-A cycle has not been done, therefore a role for TH metabolism in the regulation of  
453 the T-A cycle rather than just the overall seasonal physiology remains to be evaluated.

454 During IBE, the increased expression of Mlx, a BHLH-zip transcription factor, was of particular  
455 interest. Playing a crucial role in glucose homeostasis, MLX along with MLXIP translocates to  
456 the nucleus in response to high glucose-6-phosphate conditions, targeting glucose-sensitive  
457 genes for transcription (Stoltzman et al. 2008). One of these is Txnip, which prevents the uptake  
458 of glucose into the cell, thereby forming a negative feedback loop limiting the conversion to  
459 glucose to glucose-6-phosphate for glycolysis (Stoltzman et al. 2008). Expression of Txnip in  
460 the mediobasal hypothalamus (i.e. the tancytic region) is induced in response to fasting in  
461 mice, daily torpor in Siberian hamsters (Hand et al. 2013), torpor in the garden dormouse

462 (*Eliomys quersinus*, (Linnaeus 1766)) (Haugg et al. 2024) and the 13-lined ground squirrel  
463 (Schwartz et al. 2013). We see no change in Txnip expression in the golden hamster tanycytes  
464 despite the up-regulation of Mlx (Supplementary table 1). Recently, it was shown that MLX  
465 sequestered to lipid droplets in the cytoplasm cannot enter the nucleus in response to glucose,  
466 preventing it from exerting transcriptional effects (Mejhert et al. 2020). Tanycytes are rich in  
467 lipid droplets (reviewed in: (Rodríguez et al. 2019)), therefore, we speculate that MLX may be  
468 sequestered to lipid droplets in the IBE phase. Since golden hamsters eat in the IBE phase, this  
469 may provide a mechanism to ensure tanycytic sequestering of glucose to support glycolysis  
470 upon re-entry to torpor.

## 471 **Conclusions**

472 While RNA profiling does not permit the drawing of firm conclusions about how tanycytic  
473 function changes over the course of the hibernation season, the data we present serve a useful  
474 hypothesis-generating function for future studies. Based on our analysis, we identify the  
475 following priorities for further research: 1) defining how tanycytic sensitivity to metabolites  
476 and other extracellular signals changes over the course of the hibernation season 2)  
477 understanding how tanycytic energy metabolism changes and the relationship between this and  
478 the function of tanycytes and neighbouring hypothalamic cells and 3) understanding the causes  
479 of the dramatic changes in tanycytic IEG expression during T-A cycling and the consequences  
480 of these for tanycytic function during torpor.

## 482 **Acknowledgements**

483 We wish to acknowledge Clarisse Quignon for her help with sample collection. We are grateful  
484 to Dominique Ciocca and Sophie Foisset Reibel for teaching animal husbandry technique. We  
485 are also grateful to all the technical staff at the chronobiotron for their support. Further, we  
486 thank Stian Olsen and Anne Grethe Hestnes for invaluable technical assistance and guidance  
487 on the LASER capture microdissection instrument. Finally, VJM would like to thank Alex C.  
488 West, Gerard Clarke and Yin-Chen Hsieh for insightful comments on an early draft of the  
489 manuscript.

## 490 **Competing interests**

491 There are no competing interests.

## 492 **Funding**

493 The work was supported by grants from the Tromsø forskningsstiftelse (TFS) starter grant  
494 TFS2016SW and the TFS infrastructure grant (IS3\_17\_SW) awarded to S.H.W. It was also co-  
495 funded by the European Union (ERC, HiTime, 101086671). Views and opinions expressed are  
496 however those of the author(s) only and do not necessarily reflect those of the European Union  
497 or the European Research Council. Neither the European Union nor the granting authority can  
498 be held responsible for them. The Arctic seasonal timekeeping initiative (ASTI) grant and UiT  
499 strategic funds support D.G.H. and S.H.W.

500

## 501 **Data availability**

502 Sequencing data generated and analyzed during this study are available in the Gene expression  
503 omnibus (GEO) repository under the accession [GSE281814](https://www.ncbi.nlm.nih.gov/geo/query/acc.cgi?acc=GSE281814).

504 **References**

- 505 Bahrami, S., and Drabløs, F. 2016. Gene regulation in the immediate-early response process.  
506 *Adv. Biol. Regul.* **62**: 37–49. doi:10.1016/j.jbior.2016.05.001.
- 507 Bank, J.H.H., Cubuk, C., Wilson, D., Rijntjes, E., Kemmling, J., Markovsky, H., Barrett, P.,  
508 and Herwig, A. 2017. Gene expression analysis and microdialysis suggest hypothalamic  
509 triiodothyronine (T3) gates daily torpor in Djungarian hamsters (*Phodopus sungorus*). *J. Comp.*  
510 *Physiol. B* **187**(5–6): 857–868. Springer Berlin Heidelberg. doi:10.1007/s00360-017-1086-5.
- 511 Bank, J.H.H., Kemmling, J., Rijntjes, E., Wirth, E.K., and Herwig, A. 2015. Thyroid hormone  
512 status affects expression of daily torpor and gene transcription in Djungarian hamsters  
513 (*Phodopus sungorus*). *Horm. Behav.* **75**: 120–129. Academic Press.  
514 doi:10.1016/j.yhbeh.2015.09.006.
- 515 Barahona, M.J., Ferrada, L., Vera, M., and Nualart, F. 2024. Tanycytes release glucose using  
516 the glucose-6-phosphatase system during hypoglycemia to control hypothalamic energy  
517 balance. *Mol. Metab.* **84**(April): 101940. The Authors. doi:10.1016/j.molmet.2024.101940.
- 518 Blighe K, Rana S, L.M. 2024. EnhancedVolcano: Publication-ready volcano plots with  
519 enhanced colouring and labeling. R package version 1.22.0.
- 520 Blighe, K., and Lun, A. 2019. PCAtools: everything Principal Components Analysis.
- 521 Bolborea, M., and Dale, N. 2013. Hypothalamic tanycytes: potential roles in the control of  
522 feeding and energy balance. *Trends Neurosci.* **36**(2): 91–100. Elsevier.  
523 doi:10.1016/j.tins.2012.12.008.

- 524 Bolborea, M., Pollatzek, E., Benford, H., Sotelo-Hitschfeld, T., and Dale, N. 2020.  
525 Hypothalamic tanycytes generate acute hyperphagia through activation of the arcuate neuronal  
526 network. *Proc. Natl. Acad. Sci.* **117**(25): 14473–14481. doi:10.1073/pnas.1919887117.
- 527 Bratincsák, A., McMullen, D., Miyake, S., Tóth, Z.E., Hallenbeck, J.M., and Palkovits, M.  
528 2007. Spatial and temporal activation of brain regions in hibernation:c-fos expression during  
529 the hibernation bout in thirteen-lined ground squirrel. *J. Comp. Neurol.* **505**(4): 443–458.  
530 doi:10.1002/cne.21507.
- 531 Campbell, J.N., Macosko, E.Z., Fenselau, H., Pers, T.H., Lyubetskaya, A., Tenen, D., Goldman,  
532 M., Verstegen, A.M.J., Resch, J.M., McCarroll, S.A., Rosen, E.D., Lowell, B.B., and Tsai, L.T.  
533 2017. A molecular census of arcuate hypothalamus and median eminence cell types. *Nat.*  
534 *Neurosci.* **20**(3): 484–496. doi:10.1038/nn.4495.
- 535 Chayama, Y., Ando, L., Tamura, Y., Miura, M., and Yamaguchi, Y. 2016. Decreases in body  
536 temperature and body mass constitute pre-hibernation remodelling in the Syrian golden  
537 hamster, a facultative mammalian hibernator. *R. Soc. Open Sci.* **3**(4): 160002.  
538 doi:10.1098/rsos.160002.
- 539 Chen, Y., Lun, A.T.L., and Smyth, G.K. 2014. Differential Expression Analysis of Complex  
540 RNA-seq Experiments Using edgeR. *In* *Statistical Analysis of Next Generation Sequencing*  
541 *Data. Edited by S. Datta and D. Nettleton. Frontiers in Probability and the Statistical Sciences.*  
542 Springer, Cham. doi:10.1007/978-3-319-07212-8\_3
- 543 Chmura, H.E., Duncan, C., Saer, B., Moore, J.T., Barnes, B.M., Loren Buck, C., Christian,  
544 H.C., Loudon, A.S.I., and Williams, C.T. 2022. Hypothalamic remodeling of thyroid hormone  
545 signaling during hibernation in the arctic ground squirrel. *Commun. Biol.* **5**(1): 492.  
546 doi:10.1038/s42003-022-03431-8.

- 547 Dali, R., Estrada-Meza, J., and Langlet, F. 2023. Tanycyte, the neuron whisperer. *Physiol.*  
548 *Behav.* **263**: 114108. doi:10.1016/j.physbeh.2023.114108.
- 549 Dardente, H., Hazlerigg, D.G., and Ebling, F.J.P. 2014. Thyroid Hormone and Seasonal  
550 Rhythmicity. *Front. Endocrinol. (Lausanne)*. **5**: 19. *Frontiers*. doi:10.3389/fendo.2014.00019.
- 551 Dardente, H., Wood, S., Ebling, F., and Sáenz de Miera, C. 2019. An integrative view of  
552 mammalian seasonal neuroendocrinology. *J. Neuroendocrinol.* **31**(5): e12729.  
553 doi:10.1111/jne.12729.
- 554 Darrow, J.M., Yogeve, L., and Goldman, B.D. 1987. Patterns of reproductive hormone secretion  
555 in hibernating Turkish hamsters. *Am J Physiol Regul Integr Comp Physiol* **253**: 329–336.
- 556 Dentice, M., Bandyopadhyay, A., Gereben, B., Callebaut, I., Christoffolete, M.A., Kim, B.W.,  
557 Nissim, S., Mornon, J.-P., Zavacki, A.M., Zeöld, A., Capelo, L.P., Curcio-Morelli, C., Ribeiro,  
558 R., Harney, J.W., Tabin, C.J., and Bianco, A.C. 2005. The Hedgehog-inducible ubiquitin ligase  
559 subunit WSB-1 modulates thyroid hormone activation and PTHrP secretion in the developing  
560 growth plate. *Nat. Cell Biol.* **7**(7): 698–705. doi:10.1038/ncb1272.
- 561 Dobin, A., Davis, C.A., Schlesinger, F., Drenkow, J., Zaleski, C., Jha, S., Batut, P., Chaisson,  
562 M., and Gingeras, T.R. 2013. STAR: ultrafast universal RNA-seq aligner. *Bioinformatics*  
563 **29**(1): 15–21. doi:10.1093/bioinformatics/bts635.
- 564 Dunlap, J.C., Loros, J.J., and DeCoursey, P.J. 2004. *Chronobiology: biological timekeeping.*  
565 *Sinauer Associates*. Available from <https://psycnet.apa.org/record/2003-06316-000>.

- 566 Duquenne, M., Folgueira, C., Bourouh, C., Millet, M., Silva, A., Clasadonte, J., Imbernon, M.,  
567 Fernandois, D., Martinez-Corral, I., Kusumakshi, S., Caron, E., Rasika, S., Deliglia, E., Jouy,  
568 N., Oishi, A., Mazzone, M., Trinquet, E., Tavernier, J., Kim, Y.-B., Ory, S., Jockers, R.,  
569 Schwaninger, M., Boehm, U., Nogueiras, R., Annicotte, J.-S., Gasman, S., Dam, J., and Prévot,  
570 V. 2021. Leptin brain entry via a tanycytic LepR–EGFR shuttle controls lipid metabolism and  
571 pancreas function. *Nat. Metab.* **3**(8): 1071–1090. doi:10.1038/s42255-021-00432-5.
- 572 Ebling, F.J.P., and Lewis, J.E. 2018. Tanycytes and hypothalamic control of energy  
573 metabolism. *Glia* **66**(6): 1176–1184. doi:10.1002/glia.23303.
- 574 Ebling, F.J.P.P. 2014. On the value of seasonal mammals for identifying mechanisms  
575 underlying the control of food intake and body weight. *Horm. Behav.* **66**(1): 56–65. Elsevier  
576 B.V. doi:10.1016/j.yhbeh.2014.03.009.
- 577 Frerichs, K.U., Smith, C.B., Brenner, M., DeGracia, D.J., Krause, G.S., Marrone, L., Dever,  
578 T.E., and Hallenbeck, J.M. 1998. Suppression of protein synthesis in brain during hibernation  
579 involves inhibition of protein initiation and elongation. *Proc. Natl. Acad. Sci.* **95**(24): 14511–  
580 14516. doi:10.1073/pnas.95.24.14511.
- 581 Fu, R., Gillen, A.E., Grabek, K.R., Riemondy, K.A., Epperson, L.E., Bustamante, C.D.,  
582 Hesselberth, J.R., and Martin, S.L. 2021. Dynamic RNA Regulation in the Brain Underlies  
583 Physiological Plasticity in a Hibernating Mammal. *Front. Physiol.* **11**.  
584 doi:10.3389/fphys.2020.624677.
- 585 Gaston, S., and Menaker, M. 1967. Photoperiodic control of hamster testis. *Science* (80- ).  
586 **158**(3803): 925–928.

- 587 Ge, S.X., Jung, D., Jung, D., and Yao, R. 2020. ShinyGO: a graphical gene-set enrichment tool  
588 for animals and plants. *Bioinformatics* **36**(8): 2628–2629. Oxford Academic.  
589 doi:10.1093/BIOINFORMATICS/BTZ931.
- 590 Gius, D., Cao, X.M., Rauscher, F.J., Cohen, D.R., Curran, T., and Sukhatme, V.P. 1990.  
591 Transcriptional activation and repression by Fos are independent functions: the C terminus  
592 represses immediate-early gene expression via CArG elements. *Mol. Cell. Biol.* **10**(8): 4243–  
593 4255. doi:10.1128/MCB.10.8.4243.
- 594 Gu, Z., Eils, R., and Schlesner, M. 2016. Complex heatmaps reveal patterns and correlations in  
595 multidimensional genomic data. *Bioinformatics* **32**(18): 2847–2849.  
596 doi:10.1093/bioinformatics/btw313.
- 597 Gwinner, E. 1986. Circannual rhythms. Springer Verlag, Berlin Heidelberg.
- 598 Hand, L.E., Saer, B.R.C., Hui, S.T., Jinnah, H.A., Steinlechner, S., Loudon, A.S.I., and  
599 Bechtold, D.A. 2013. Induction of the metabolic regulator txnip in fasting-induced and natural  
600 torpor. *Endocrinology* **154**(6): 2081–2091. doi:10.1210/en.2012-2051.
- 601 Hanon, E.A., Lincoln, G.A., Fustin, J.-M., Dardente, H., Masson-Pévet, M., Morgan, P.J., and  
602 Hazlerigg, D.G. 2008. Ancestral TSH mechanism signals summer in a photoperiodic mammal.  
603 *Curr. Biol.* **18**(15): 1147–52. doi:10.1016/j.cub.2008.06.076.
- 604 Hanon, E.A., Routledge, K., Dardente, H., Masson-Pévet, M., Morgan, P.J., and Hazlerigg,  
605 D.G. 2010. Effect of photoperiod on the thyroid-stimulating hormone neuroendocrine system  
606 in the European hamster (*Cricetus cricetus*). *J. Neuroendocrinol.* **22**(1): 51–5.  
607 doi:10.1111/j.1365-2826.2009.01937.x.

- 608 Haque, M., Kendal, J.K., MacIsaac, R.M., and Demetrick, D.J. 2016. WSB1: from homeostasis  
609 to hypoxia. *J. Biomed. Sci.* **23**(1): 61. doi:10.1186/s12929-016-0270-3.
- 610 Haugg, E., Borner, J., Diedrich, V., and Herwig, A. 2022. Comparative transcriptomics of the  
611 Djungarian hamster hypothalamus during short photoperiod acclimation and spontaneous  
612 torpor. *FEBS Open Bio* **12**(2): 443–459. doi:10.1002/2211-5463.13350.
- 613 Haugg, E., Borner, J., Stalder, G., Küber-Heiss, A., Giroud, S., and Herwig, A. 2024.  
614 Comparative transcriptomics of the garden dormouse hypothalamus during hibernation. *FEBS*  
615 *Open Bio* **14**(2): 241–257. doi:10.1002/2211-5463.13731.
- 616 Hazlerigg, D., and Simonneaux, V. 2015. Seasonal reproduction in mammals. In Knobil and  
617 Neill's physiology and reproduction, 4th edition. Edited by T. Plant and A. Zeleznic. Academic  
618 Press. pp. 1575–1660.
- 619 Hazlerigg, D.G., Appenroth, D., Tomotani, B.M., West, A.C., and Wood, S.H. 2023. Biological  
620 timekeeping in polar environments: lessons from terrestrial vertebrates. *J. Exp. Biol.* **226**(23).  
621 doi:10.1242/jeb.246308.
- 622 Hofmann, K., Lamberz, C., Piotrowitz, K., Offermann, N., But, D., Scheller, A., Al-Amoudi,  
623 A., and Kuerschner, L. 2017. Tanycytes and a differential fatty acid metabolism in the  
624 hypothalamus. *Glia* **65**(2): 231–249. doi:10.1002/glia.23088.
- 625 Hut, R.A.A., Dardente, H., and Riede, S.J.J. 2014. Seasonal Timing: How Does a Hibernator  
626 Know When to Stop Hibernating? *Curr. Biol.* **24**(13): R602–R605. Cell Press.  
627 doi:10.1016/j.cub.2014.05.061.

- 628 Johnson, R.J., Stenvinkel, P., Andrews, P., Sánchez-Lozada, L.G., Nakagawa, T., Gaucher, E.,  
629 Andres-Hernando, A., Rodriguez-Iturbe, B., Jimenez, C.R., Garcia, G., Kang, D.H., Tolan,  
630 D.R., and Lanaspá, M.A. 2020. Fructose metabolism as a common evolutionary pathway of  
631 survival associated with climate change, food shortage and droughts. *J. Intern. Med.* **287**(3):  
632 252–262. doi:10.1111/joim.12993.
- 633 Kanehisa, M., Goto, S. 2000. KEGG: Kyoto Encyclopedia of Genes and Genomes, *Nucleic*  
634 *Acids Res* **28**(1):27–30, doi:10.1093/nar/28.1.27.
- 635 Klosen, P., Sébert, M.-E., Rasri, K., Laran-Chich, M.-P., and Simonneaux, V. 2013. TSH  
636 restores a summer phenotype in photoinhibited mammals via the RF-amides RFRP3 and  
637 kisspeptin. *FASEB J.* **27**(7): 2677–86. doi:10.1096/fj.13-229559.
- 638 Langlet, F. 2014. Tanycytes: A Gateway to the Metabolic Hypothalamus. *J. Neuroendocrinol.*  
639 **26**(11): 753–760. doi:10.1111/jne.12191.
- 640 Lara Aparicio, S.Y., Laureani Fierro, Á. de J., Aranda Abreu, G.E., Toledo Cárdenas, R., García  
641 Hernández, L.I., Coria Ávila, G.A., Rojas Durán, F., Aguilar, M.E.H., Manzo Denes, J., Chi-  
642 Castañeda, L.D., and Pérez Estudillo, C.A. 2022. Current Opinion on the Use of c-Fos in  
643 Neuroscience. *NeuroSci* **3**(4): 687–702. doi:10.3390/neurosci3040050.
- 644 Lewis, J.E., and Ebling, F.J.P. 2017. Tanycytes As Regulators of Seasonal Cycles in  
645 Neuroendocrine Function. *Front. Neurol.* **8**: 79. *Frontiers*. doi:10.3389/fneur.2017.00079.
- 646 Lhomme, T., Clasadonte, J., Imbernon, M., Fernandois, D., Sauve, F., Caron, E., da Silva Lima,  
647 N., Heras, V., Martinez-Corral, I., Mueller-Fielitz, H., Rasika, S., Schwaninger, M., Nogueiras,  
648 R., and Prevot, V. 2021. Tanycytic networks mediate energy balance by feeding lactate to  
649 glucose-insensitive POMC neurons. *J. Clin. Invest.* **131**(18). doi:10.1172/JCI140521.

- 650 Logan, S.M., Wu, C.-W., and Storey, K.B. 2019. The squirrel with the lagging eIF2: Global  
651 suppression of protein synthesis during torpor. *Comp. Biochem. Physiol. Part A Mol. Integr.*  
652 *Physiol.* **227**: 161–171. doi:10.1016/j.cbpa.2018.10.014.
- 653 Lyman, C.P., Willis, J., Malan, A., and Wang, L.C.. 1982. Hibernation and torpor in mammals  
654 and birds. Edited By C.P. Lyman. Academic Press, New York.
- 655 Maistrovski, Y., Biggar, K.K., and Storey, K.B. 2012. HIF-1 $\alpha$  regulation in mammalian  
656 hibernators: role of non-coding RNA in HIF-1 $\alpha$  control during torpor in ground squirrels and  
657 bats. *J. Comp. Physiol. B* **182**(6): 849–859. doi:10.1007/s00360-012-0662-y.
- 658 Markussen, F.A.F., Cázarez-Márquez, F., Melum, V.J., Hazlerigg, D., and Wood, S. 2024. C-  
659 Fos Induction in the Choroid Plexus, Tanycytes and Pars Tuberalis Is an Early Indicator of  
660 Spontaneous Arousal From Torpor in a Deep Hibernator. *J. Exp. Biol.* doi:10.1242/jeb.247224.
- 661 McCarthy, D.J., Chen, Y., and Smyth, G.K. 2012. Differential expression analysis of  
662 multifactor RNA-Seq experiments with respect to biological variation. *Nucleic Acids Res.*: 1–  
663 10. doi:10.1093/nar/gks042.
- 664 Mejhert, N., Kuruvilla, L., Gabriel, K.R., Elliott, S.D., Guie, M.-A., Wang, H., Lai, Z.W., Lane,  
665 E.A., Christiano, R., Danial, N.N., Farese, R. V., and Walther, T.C. 2020. Partitioning of MLX-  
666 Family Transcription Factors to Lipid Droplets Regulates Metabolic Gene Expression. *Mol.*  
667 *Cell* **77**(6): 1251-1264.e9. doi:10.1016/j.molcel.2020.01.014.
- 668 Melum, V.J., Sáenz de Miera, C., Markussen, F.A.F., Cázarez-Márquez, F., Jaeger, C., Sandve,  
669 S.R., Simonneaux, V., Hazlerigg, D.G., and Wood, S.H. 2024. Hypothalamic tanycytes as  
670 mediators of maternally programmed seasonal plasticity. *Curr. Biol.* **34**(3): 632-640.e6. *Cell*  
671 *Press.* doi:10.1016/J.CUB.2023.12.042.

- 672 Milesi, S., Simonneaux, V., and Klosen, P. 2017. Downregulation of Deiodinase 3 is the earliest  
673 event in photoperiodic and photorefractory activation of the gonadotropic axis in seasonal  
674 hamsters. *Sci. Rep.* **7**(1): 17739. doi:10.1038/s41598-017-17920-y.
- 675 Morin, L.P., and Zucker, I. 1978. Photoperiodic regulation of copulatory behaviour in the male  
676 hamster. *J. Endocrinol.* **77**(2): 249–258. *J Endocrinol.* doi:10.1677/JOE.0.0770249.
- 677 Murphy, M., Jethwa, P.H., Warner, A., Barrett, P., Nilaweera, K.N., Brameld, J.M., and Ebling,  
678 F.J.P. 2012. Effects of Manipulating Hypothalamic Triiodothyronine Concentrations on  
679 Seasonal Body Weight and Torpor Cycles in Siberian Hamsters. *Endocrinology* **153**(1): 101–  
680 112. doi:10.1210/en.2011-1249.
- 681 Nilaweera, K., Herwig, A., Bolborea, M., Campbell, G., Mayer, C.D., Morgan, P.J., Ebling,  
682 F.J.P., and Barrett, P. 2011. Photoperiodic regulation of glycogen metabolism, glycolysis, and  
683 glutamine synthesis in tanycytes of the Siberian hamster suggests novel roles of tanycytes in  
684 hypothalamic function. *Glia* **59**(11): 1695–1705. doi:10.1002/glia.21216.
- 685 Parkash, J., Messina, A., Langlet, F., Cimino, I., Loyens, A., Mazur, D., Gallet, S., Balland, E.,  
686 Malone, S.A., Pralong, F., Cagnoni, G., Schellino, R., De Marchis, S., Mazzone, M.,  
687 Pasterkamp, R.J., Tamagnone, L., Prevot, V., and Giacobini, P. 2015. Semaphorin7A regulates  
688 neuroglial plasticity in the adult hypothalamic median eminence. *Nat. Commun.* **6**: 6385.  
689 doi:10.1038/ncomms7385.
- 690 Pasquettaz, R., Kolotuev, I., Rohrbach, A., Gouelle, C., Pellerin, L., and Langlet, F. 2021.  
691 Peculiar protrusions along tanycyte processes face diverse neural and nonneural cell types in  
692 the hypothalamic parenchyma. *J. Comp. Neurol.* **529**(3): 553–575. doi:10.1002/cne.24965.

- 693 Prevot, V., Dehouck, B., Sharif, A., Ciofi, P., Giacobini, P., and Clasadonte, J. 2018. The  
694 Versatile Tanycyte: A Hypothalamic Integrator of Reproduction and Energy Metabolism.  
695 *Endocr. Rev.* **39**(3): 333–368. doi:10.1210/er.2017-00235.
- 696 Revel, F.G., Saboureau, M., Pévet, P., Mikkelsen, J.D., and Simonneaux, V. 2006. Melatonin  
697 regulates type 2 deiodinase gene expression in the Syrian hamster. *Endocrinology* **147**(10):  
698 4680–7. doi:10.1210/en.2006-0606.
- 699 Rizzoti, K., and Lovell-Badge, R. 2017. Pivotal role of median eminence tanycytes for  
700 hypothalamic function and neurogenesis. *Mol. Cell. Endocrinol.* **445**: 7–13. Elsevier.  
701 doi:10.1016/J.MCE.2016.08.020.
- 702 Rodríguez, E., Guerra, M., Peruzzo, B., and Blázquez, J.L. 2019. Tanycytes: A rich  
703 morphological history to underpin future molecular and physiological investigations. *J.*  
704 *Neuroendocrinol.* **31**(3). doi:10.1111/jne.12690.
- 705 Ruf, T., and Geiser, F. 2015. Daily torpor and hibernation in birds and mammals. *Biol. Rev.*  
706 **90**(3): 891–926. doi:10.1111/brv.12137.
- 707 Sáenz de Miera, C., Hanon, E.A., Dardente, H., Birnie, M., Simonneaux, V., Lincoln, G.A., and  
708 Hazlerigg, D.G. 2013. Circannual variation in thyroid hormone deiodinases in a short-day  
709 breeder. *J. Neuroendocrinol.* **25**(4): 412–21. doi:10.1111/jne.12013.
- 710 Sáenz de Miera, C., Monecke, S., Bartzen-Sprauer, J., Laran-Chich, M.-P., Pévet, P., Hazlerigg,  
711 D.G., and Simonneaux, V. 2014. A Circannual Clock Drives Expression of Genes Central for  
712 Seasonal Reproduction. *Curr. Biol.* **24**(13): 1500–1506. doi:10.1016/j.cub.2014.05.024.

- 713 Sano, Y., Shiina, T., Naitou, K., Nakamori, H., and Shimizu, Y. 2015. Hibernation-specific  
714 alternative splicing of the mRNA encoding cold-inducible RNA-binding protein in the hearts  
715 of hamsters. *Biochem. Biophys. Res. Commun.* **462**(4): 322–325. *Biochem Biophys Res*  
716 *Commun.* doi:10.1016/J.BBRC.2015.04.135.
- 717 Schou, K.B., Pedersen, L.B., and Christensen, S.T. 2015. Ins and outs of GPCR signaling in  
718 primary cilia. *EMBO Rep.* **16**(9): 1099–1113. doi:10.15252/embr.201540530.
- 719 Schwartz, C., Hampton, M., and Andrews, M.T. 2013. Seasonal and Regional Differences in  
720 Gene Expression in the Brain of a Hibernating Mammal. *PLoS One* **8**(3): e58427. Public  
721 Library of Science. doi:10.1371/journal.pone.0058427.
- 722 Shearer, K.D., Goodman, T.H., Ross, A.W., Reilly, L., Morgan, P.J., and McCaffery, P.J. 2010.  
723 Photoperiodic regulation of retinoic acid signaling in the hypothalamus. *J. Neurochem.* **112**(1):  
724 246–257. doi:10.1111/j.1471-4159.2009.06455.x.
- 725 Stoltzman, C.A., Peterson, C.W., Breen, K.T., Muoio, D.M., Billin, A.N., and Ayer, D.E. 2008.  
726 Glucose sensing by MondoA:MLX complexes: A role for hexokinases and direct regulation of  
727 thioredoxin-interacting protein expression. *Proc. Natl. Acad. Sci.* **105**(19): 6912–6917.  
728 doi:10.1073/pnas.0712199105.
- 729 Vermillion, K.L., Anderson, K.J., Hampton, M., and Andrews, M.T. 2015. Gene expression  
730 changes controlling distinct adaptations in the heart and skeletal muscle of a hibernating  
731 mammal. *Physiol. Genomics* **47**(3): 58–74. doi:10.1152/physiolgenomics.00108.2014.

- 732 Wickham, H., Averick, M., Bryan, J., Chang, W., McGowan, L., François, R., Grolemund, G.,  
733 Hayes, A., Henry, L., Hester, J., Kuhn, M., Pedersen, T., Miller, E., Bache, S., Müller, K.,  
734 Ooms, J., Robinson, D., Seidel, D., Spinu, V., Takahashi, K., Vaughan, D., Wilke, C., Woo, K.,  
735 and Yutani, H. 2019. Welcome to the Tidyverse. *J. Open Source Softw.* **4**(43): 1686. The Open  
736 Journal. doi:10.21105/JOSS.01686.
- 737 Williams, D.R., Epperson, L.E., Li, W., Hughes, M.A., Taylor, R., Rogers, J., Martin, S.L.,  
738 Cossins, A.R., and Gracey, A.Y. 2005. Seasonally hibernating phenotype assessed through  
739 transcript screening. *Physiol. Genomics* **24**(1): 13–22.  
740 doi:10.1152/physiolgenomics.00301.2004.
- 741 Wood, S.H., Hindle, M.M., Mizoro, Y., Cheng, Y., Saer, B.R.C., Miedzinska, K., Christian,  
742 H.C., Begley, N., McNeilly, J., McNeilly, A.S., Meddle, S.L., Burt, D.W., and Loudon, A.S.I.  
743 2020. Circadian clock mechanism driving mammalian photoperiodism. *Nat. Commun.* **11**(1):  
744 4291. doi:10.1038/s41467-020-18061-z.
- 745 Zavacki, A.M., Arrojo e Drigo, R., Freitas, B.C.G., Chung, M., Harney, J.W., Egri, P.,  
746 Wittmann, G., Fekete, C., Gereben, B., and Bianco, A.C. 2009. The E3 Ubiquitin Ligase TEB4  
747 Mediates Degradation of Type 2 Iodothyronine Deiodinase. *Mol. Cell. Biol.* **29**(19): 5339–  
748 5347. doi:10.1128/MCB.01498-08.
- 749 Zhou, X., Lindsay, H., and Robinson, M.D. 2014. Robustly detecting differential expression in  
750 RNA sequencing data using observation weights. *Nucleic Acids Res.* **42**(11): e91.  
751 doi:10.1093/nar/gku310.  
752

753 **Figure legends**

754 **Figure 1: Photoperiod driven initiation and spontaneous termination of hibernation in**  
755 **golden hamsters (*Mesocricetus auratus*) relates to tanycyte transcriptional profile**

756 **A)** Illustration of the experimental set-up and characteristic animal behaviour in response  
757 to shifting from long photoperiod 22°C (LP, 14 hours of light, 10 hours of dark) –  
758 summer like state, to short photoperiod (SP, 10 hours of light 14 hours of dark) and cold  
759 (8°C) – initiation of Autumn/Winter programme, followed by the eventual anticipation  
760 and initiation of Spring/Summer programme. Representative core body temperature  
761 ( $T_b$ ) measurements are shown in parallel illustrate the physiological groups sampled in  
762 the experiment.  $T_b$  indicated in yellow relates to animals at LP 22°C, and  $T_b$  in blue  
763 relates to animals at SP 8°C. Ambient temperature ( $T_a$ ) of the room is denoted by the  
764 grey dotted line. Pre-hib = Pre-hibernator 4 weeks after SP 8°C, Late pre-hib = pre-  
765 hibernator 8 to 12 weeks after SP 8°C, IBE = inter-bout euthermic. Hamster images  
766 were redrawn from [https://commons.wikimedia.org/wiki/File:201606\\_hamster.png](https://commons.wikimedia.org/wiki/File:201606_hamster.png)  
767 under the [Creative Commons Attribution 4.0 International](https://creativecommons.org/licenses/by/4.0/) license.  
768 Attribution: [DBCLS](https://commons.wikimedia.org/wiki/File:201606_hamster.png).

769 **B)** Mean euthermic core body temperature ( $T_b$ ) throughout the experimental conditions.  
770 Each dot represents each individual mean euthermic  $T_b$  defined as each experimental  
771 group listed on the x-axis. For this analysis the refractory group was split into Refr. 0,  
772 1 and 2 representing weeks after last torpor bout. Results of one-way ANOVA indicate  
773 a difference between the group mean  $T_b$  ( $F_{(6, 45)} = 78.66, p < 0.0001$ ). For **B, C, D, E** –  
774 The Tukey test determined the significant pairwise differences, indicated by different  
775 letters on the plot. LP = long photoperiod, pre-hib = Pre-hibernator 4 weeks after SP  
776 8°C, L. pre-hib = pre-hibernator 8 to 12 weeks after SP 8°C, IBE = inter-bout euthermic,  
777 Refr. = refractory.

- 778 C) Each dot indicates each individual visible dissected interscapular brown adipose tissue  
 779 (iBAT) mass in grams (y-axis) for the experimental groups (x-axis). Results of one-way  
 780 ANOVA indicate a group mean difference in iBAT amount ( $F_{(5,30)}=7.245$ ,  $p<0.0001$ ).
- 781 D) Each dot represents individual testes mass in grams for each experimental group at  
 782 sampling. Results from one-way ANOVA indicate a difference between the group mean  
 783 in testis mass ( $F_{(5,30)}=134.8$ ,  $p<0.0001$ ).
- 784 E) Blood plasma levels of testosterone. Each dot is each individual's testosterone levels  
 785 (ng/ml) for the experimental group indicated on the x-axis. Results from one-way  
 786 ANOVA indicate a difference between the group mean in plasma testosterone levels  
 787 ( $F_{(5, 30)}=25.91$ ,  $p<0.0001$ ).
- 788 F) Diagram to show the workflow from frozen whole brain through frozen cryosections to  
 789 LASER Capture Microdissection (LCMD) of the ependymal layer of the tuberal part of  
 790 the 3<sup>rd</sup> Ventricle (3V), which were further processed for Illumina RNA-seq.
- 791 G) Principal component analysis of differentially expressed genes (DEG) across the  
 792 euthermic time points. The % variation contributing to each principle component (PC)  
 793 are indicated on the x and y axis. The reproductively active animals, long photoperiod  
 794 (LP) and refractory group together. The animals preparing for hibernation, pre-  
 795 hibernation (pre-hib) and late pre-hibernation (late pre-hib) separate from the animals  
 796 that have entered hibernation and are interbout euthermic, IBE). SP = short photoperiod.

797 **Figure 2: Changes in ciliary genes and the glycolytic pathway in tanycytes defines the**  
 798 **seasonal response to short photoperiod**

- 799 A) Heatmap of seasonal DEGs ( $n= 2291$ ) with k-means clustering into 5 clusters. Next to  
 800 each cluster is a normalized counts per million (cpm) plot for all genes within each  
 801 cluster to indicate direction of change between the groups as listed on the x-axis. Shown

- 802 as cluster mean normalised cpm (black line), shading  $\pm$  Standard deviation and certain  
803 genes of interest color-coded as indicated.
- 804 **B)** Dot plot of enriched pathway for genes in the respective clusters using shinyGO analysis,  
805 both KEGG and reactome database results are shown. Size of dot represent number of  
806 genes. The colour of the dot represent  $-\log_{10}$  transformed False discovery rate (*FDR*)  
807 value. The x-axis is the fold enrichment.
- 808 **C)** Specific GOterm enrichment for the genes in cluster 2. Size of dot represent number of  
809 genes. The colour of the dot represent  $-\log_{10}$  transformed *FDR* value. The x-axis is the  
810 fold enrichment.
- 811 **D)** Cellular metabolic map of the glycolytic pathway, with the differentially expressed genes  
812 color-coded as indicated.

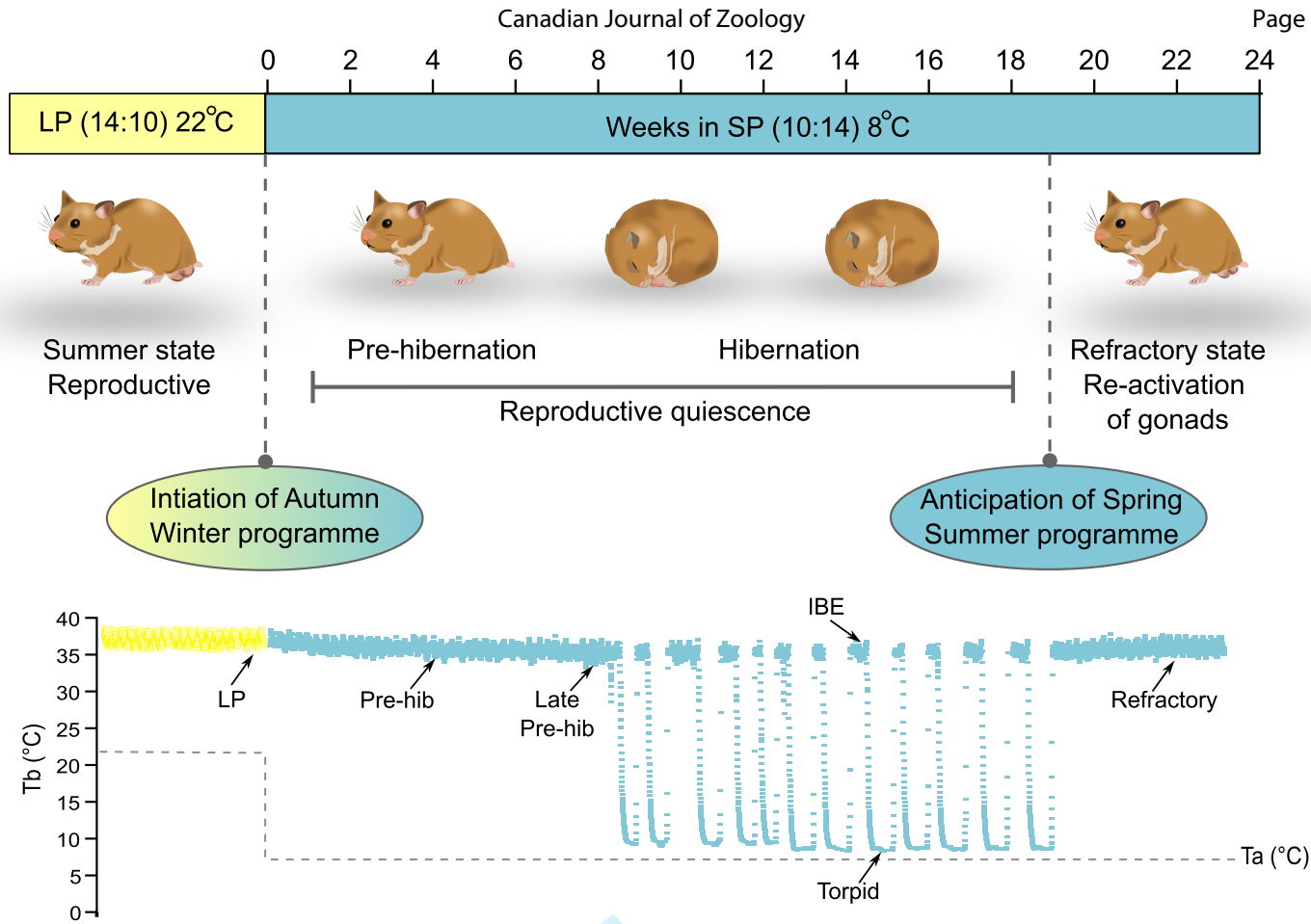
813 **Figure 3: Increased immediate early gene expression and RNA splicing in the tanyctytic**  
814 **region of torpid animals**

- 815 **A)** Representative illustration of the core body temperature ( $T_b$ ) recordings of an animal  
816 cycling from torpor to the interbout euthermic state and back again to torpor. Days spent  
817 in short photoperiod denoted on the x-axis.
- 818 **B)** Volcano plot for gene expression changes between interbout euthermic (IBE) and  
819 torpor. Dotted horizontal line indicate the false discovery rate, *FDR*= 0.05 threshold;  
820 Data are presented as  $\log_2$  fold change, increased in inter bout euthermic (IBE) in red,  
821 increased in torpor in blue, genes with an *FDR*>0.05 are shown in green.
- 822 **C)** Counts per million plots across all samples for Fos, Wsb1, Eif5, Mlx. Each dot  
823 represents an individual count per million defined as each experimental group listed on  
824 the x-axis. A generalized linear model (GLM) analysis was used to assess the group  
825 mean gene expression differences (all genes had an *FDR* less than 0.0001); specific  
826 statistical values are in supplementary table 1.

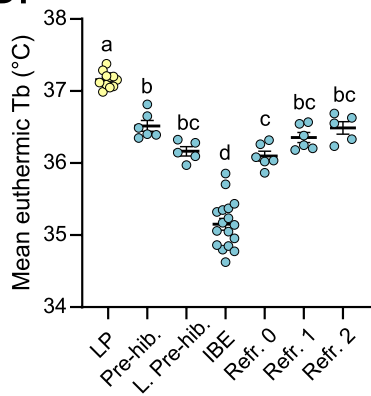
- 827 **D)** Dot plot of enriched pathways for genes increased in torpor using shinyGO analysis,  
828 both Kyoto encyclopedia of genes and genomes (KEGG) and reactome database results  
829 are shown. Size of dot represent number of genes. The colour of the dot represent  $-\log_{10}$   
830 transformed *FDR* value. The x-axis is the fold enrichment.
- 831 **E)** Dot plot of enriched pathways for genes increased in interbout euthermic (IBE) using  
832 shinyGO analysis, both Kyoto encyclopedia of genes and genomes (KEGG) and  
833 reactome database results are shown. Size of dot represent number of genes. The colour  
834 of the dot represent  $-\log_{10}$  transformed *FDR* value. The x-axis is the fold enrichment.

Draft

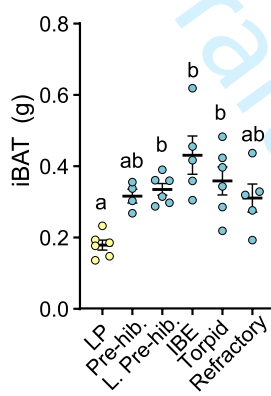
A.



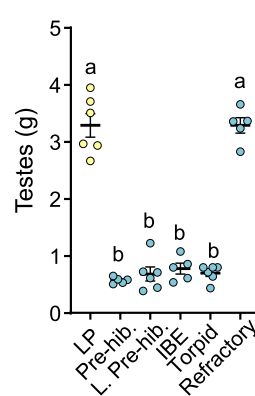
B.



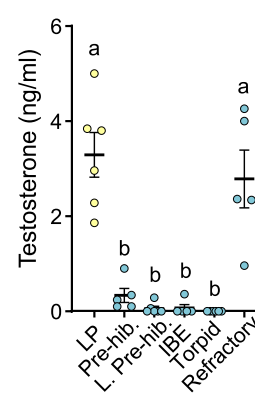
C.



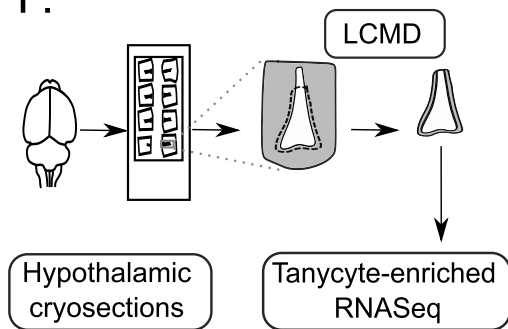
D.



E.



F.



G.

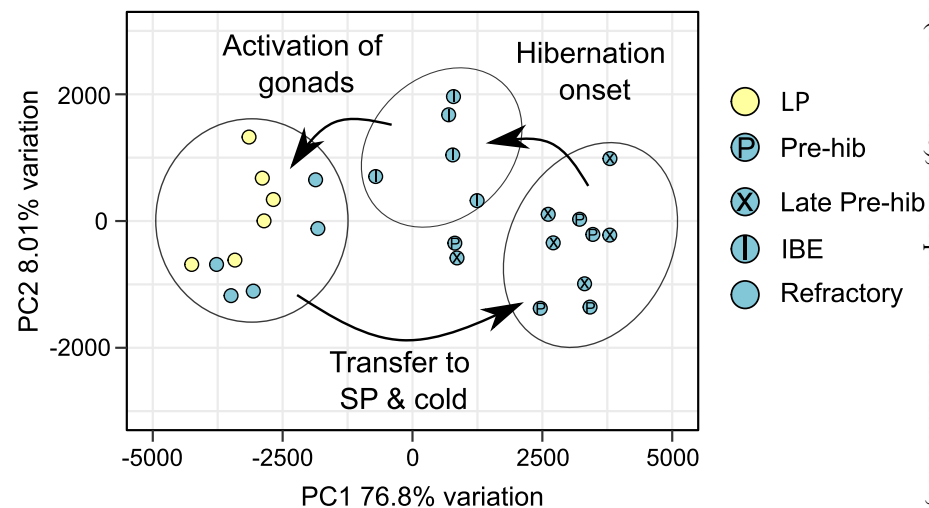
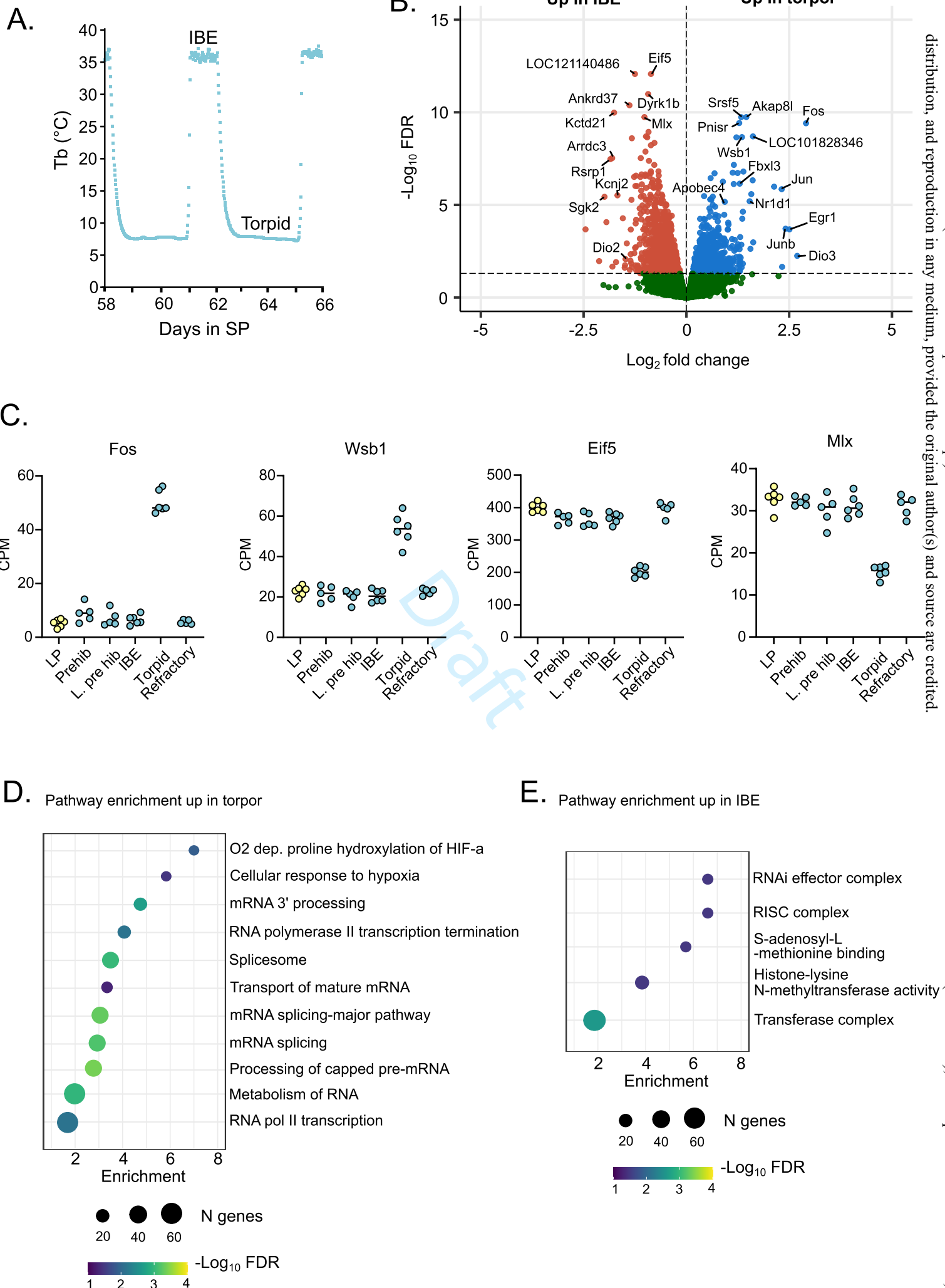


Figure 1





OPEN ACCESS: This work (the Author's Accepted Manuscript) is licensed under a Creative Commons Attribution 4.0 International License (CC BY 4.0), which permits unrestricted use, distribution, and reproduction in any medium, provided the original author(s) and source are credited.

Figure 3